



Cite this: RSC Adv., 2019, 9, 30534

Received 14th August 2019
 Accepted 20th September 2019

DOI: 10.1039/c9ra06363c

rsc.li/rsc-advances

1. Introduction

Due to its appropriate optical band gap, high optical absorption coefficient, good ion migration ability and long carrier life, organic-inorganic hybrid perovskite is considered as an ideal material for use in the light absorption layer of solar cells.^{1–5} In the past decade, new breakthroughs have been made in the research of perovskite solar cells (PSCs).^{6–8} So far, the highest power conversion efficiency (PCE) of organic-inorganic hybrid perovskite solar cells has reached 25.2%,⁹ which is higher than the efficiency of commercial silicon solar cells. However, the poor long-term stability seriously limits the large-scale commercial use of organic-inorganic hybrid perovskite solar cells.^{10–12} Although some studies have effectively improved the stability of hybrid perovskite solar cells,^{13,14} they still cannot meet the requirements for practical applications. But the all-inorganic halide perovskite with good thermal stability can be obtained by completely replacing the organic components (MA^+ , FA^+) of mixed perovskite with Cs^+ .¹⁵

Typical all-inorganic halide perovskite materials mainly include $CsPbI_3$,¹⁶ $CsPbI_2Br$,¹⁷ $CsPbBr_3$ (ref. 18) and $CsSnI_3$.¹⁹ Among them, $CsPbI_3$ and $CsPbI_2Br$ of cubic phase have appropriate optical band gaps, 1.73 eV and 1.92 eV, respectively.^{16,20} Therefore, these two halide perovskites have been extensively studied and the PCE of devices has been rapidly improved.²⁰ Nevertheless, there is still a big

^aTsinghua-Berkeley Shenzhen Institute (TBSI), Tsinghua University, Shenzhen, 518000, China. E-mail: weiguodan@sz.tsinghua.edu.cn; fykang@sz.tsinghua.edu.cn

^bTsinghua Shenzhen International Graduate School, Tsinghua University, Shenzhen, 518000, China

^cSchool of Materials Science and Engineering, Tsinghua University, Beijing 100084, China

† Fang He and Wenzhan Xu are contributed equally to this work.

Highly crystalline $CsPbI_2Br$ films for efficient perovskite solar cells via compositional engineering

Fang He,^{†,ab} Wenzhan Xu,^{†,ab} Meng Zhang,^{ab} Xuan Zhang,^{ab} Baofu Ding,^{ab} Guodan Wei,^{ID,ab} and Feiyu Kang,^{*abc}

All-inorganic $CsPbI_2Br$ shows high thermal stability for promising application in perovskite solar cells (PSCs). The performance of PSCs is significantly affected by their morphology and crystallinity induced by compositional ratio, solvent/anti-solvent engineering and post thermal annealing. In this study, the compositional ratio effect of two precursors, PbI_2 and $CsBr$, on the power conversion efficiency (PCE) of a device with $ITO/SnO_2/CsPbI_2Br/Spiro-MeOTAD/Au$ structure was investigated. With the assistance of anti-solvent chlorobenzene, perovskite with a $PbI_2 : CsBr$ ratio of 1.05 : 1 showed a high quality thin film with higher crystallinity and larger grain size. In addition, the molar ratio of precursors PbI_2 and $CsBr$ improved the PCE of the PSCs, and the PSCs fabricated using the perovskite with an optimal ratio of PbI_2 and $CsBr$ exhibited a PCE of 13.34%.

gap between the current maximum efficiency and the theoretical schottky limit,²⁰ which suggests that the all-inorganic perovskite solar cells still have great room for improvement and research value in photoelectric conversion efficiency. On the other hand, the all-inorganic halide perovskite usually suffers a severe phase transition problem. In ambient air environment, $CsPbI_3$ and $CsPbI_2Br$ of cubic phase are easily converted into non-perovskite phase, which will seriously affect their photoelectric performance and practical utilization of devices.²¹

Studies have shown that, compared with $CsPbI_3$, $CsPbI_2Br$ is easier to maintain the cubic phase structure, which has intrigued great attention.²² Chen *et al.* confirmed that the a-phase and b-phase $CsPbI_2Br$ have better thermal stability and phase stability than $CsPbI_3$ due to the mixing of halide elements through theoretical calculations.²³ Through interface engineering,²⁴ solvent engineering,²⁵ precursor engineering²⁶ and other strategies, the photoelectric performance of $CsPbI_2Br$ has been effectively improved. For example, Guo *et al.*²⁷ successfully synthesized Rb-doped $CsPbI_2Br$ film with improved crystallinity and light absorption. Based on this, the prepared all-inorganic perovskite solar cells without hole transport layer achieved stabilized PCE of over 11%. Bai *et al.*²⁸ improved the crystallinity of the $CsPbBrI_2$ film by preheating the precursor solution at 100 °C, and reached a high efficiency of up to 14.81% with the device structure of $FTO/TiO_2/CsPbBrI_2/CsPbBrI_2$ QDs/PTAA/Au. Chen *et al.*²⁹ precisely controlled the growth of α - $CsPbI_2Br$ crystal by the synergistic effect of gradient thermal annealing and anti-solvent method, and obtained a high-quality film with few defects and good stability, achieving a record PCE of 16.07%. Liu *et al.*³⁰ successfully designed a novel structure of solar cell by using $ZnO@C_{60}$ bilayer as the electron transport layer, achieving a high PCE of 13.3% with good thermal



stability. Dong *et al.*³¹ used EtOH anti-solvent and optimized CsBr deposition cycle to obtain a high-purity phase and high-quality CsPbI₂Br film, successfully achieving a record PCE of 10.21% for the α -CsPbI₂Br PSCs without hole transporting material.

Herein, we studied the effect of raw material stoichiometric ratio on the properties of CsPbI₂Br. Four perovskite solar cells with ITO/SnO₂/CsPbI₂Br/Spiro-MeOTAD/Au were fabricated by changing the molar ratios of PbI₂ and CsBr (0.95 : 1, 1.00 : 1, 1.05 : 1, 1.10 : 1). We found that excessive PbI₂ would lead to obvious PbI₂ peak in the XRD pattern, and a small amount of PbI₂ would significantly affect the morphology and crystallinity of as-prepared CsPbI₂Br perovskite films. In addition, different proportions of PbI₂ and CsBr will also lead to changes in optical band gap and light absorption properties of perovskite thin films, as well as differences in CsPbI₂Br phase stability. Our results show that solar cell devices have the best power conversion efficiency when the molar ratio of PbI₂ and CsBr is 1.05 : 1. The enhanced PCE originates from the higher crystallinity and defects-free of perovskite thin film with appropriate grain size characterized by X-ray diffraction (XRD) and can electronic microscopy (SEM).

2. Experimental

2.1 Materials

Lead iodide (PbI₂, 99.999%) and tin(IV) oxide (SnO₂) colloid precursor were purchased from Alfa Aesar; cesium bromide (CsBr, 99.999%), chlorobenzene (CB, 99.8%), anhydrous dimethyl sulfoxide (DMSO, \geq 99.9%), *N,N*-dimethylformamide (DMF, 99.8%), 4-*tert*-butylpyridine (*t*BP), tris(2-(1*H*-pyrazol-1-yl)-4-*tert*-butylpyridine) cobalt(III)-tris(bis(trifluoromethylsulfonyl) imide) (FK209) and bis(trifluoromethylsulfonyl)amine lithium salt (Li-TFSI) were purchased from Sigma Aldrich. Anhydrous methanol, ethanol (>99.5%) and isopropyl alcohol (IPA, 99.5%) were purchased from Acros; Spiro-MeOTAD (99.8%) was purchased from Xi'an Polymer Light Technology Corp. All materials and reagents were used as received without further purification.

2.2 Precursor preparation

1 M CsBr and X M PbI₂ ($X = 0.95, 1.00, 1.05, 1.10$) were dissolved in a mixed solvent (DMSO : DMF = 9 : 1) according to certain stoichiometric ratios, and stirred at 70 °C for 12 h. The CsPbI₂Br precursor solution was then obtained by filtration through a 0.22 μ m PTFE filter.

2.3 Solar cells fabrication

The ITO glasses were successively cleaned with acetone, ethanol and deionized water respectively by ultrasonic cleaning for 15 minutes, respectively. Before the spin coating, each ITO glass was blown dry with nitrogen gun and cleaned with plasma for 60 s. SnO₂ was selected as the electron transport layer. We diluted the SnO₂ colloid precursor to 5% with deionized water, then spin-coated at 3000 rpm for 30 s, and thermal annealed at 150 °C for 30 min to obtain an electron transport layer. Then the 1 M CsPbI₂Br precursor solution was deposited on the SnO₂

layer at the speed of 1000 rpm for 10 s and 4500 rpm for 35 s in a glove box, annealing at 260 °C for 10 minutes. For deposition of hole-transporting material, Spiro-MeOTAD was dissolved in chlorobenzene with a concentration of 80 mg mL⁻¹, then 35 μ L of lithium bis (trifluoromethanesulfonyl)imide in acetonitrile (260 mg mL⁻¹) and 30 μ L of 4-*tert*-butylpyridine was added into the Spiro-MeOTAD solution. The mixture was coated onto the perovskite film at 3500 RPM for 30 s to form a Spiro-MeOTAD hole-transporting layer. Finally, the counter electrode was deposited by thermal evaporation of 80 nm-thick gold under a pressure of 2×10^{-6} mbar. The active area was measured to be 0.045 cm².

2.4 Characterization of perovskite thin films

UV-vis absorption and photoluminescence (PL) spectra of thin films were recorded on a HP 8453 spectrophotometer and FLS920 spectrofluorimeter (Edinburgh Instruments), respectively. A 150 W, ozone-free xenon arc lamp was used in PL measurements. Scanning electron microscope (SEM) images were obtained by using a field emission scanning electron microscope (JEOL-7401). Thicknesses of thin films were measured by Dektak 150 surface profilometer. X-Ray Diffraction (XRD) patterns were measured by an X-ray diffractometer Bruker D8 Advance using Cu K α radiation source with a scan rate of 10° min⁻¹.

2.5 Characterization of perovskite solar cells

The *J-V* characteristics of PSCs were measured by a Keithley model 2400 source measure unit (Newport, Oriel AM 1.5 G, 100 mW cm⁻²). The light intensity of 100 mW cm⁻² was calibrated by a silicon reference cell. The external quantum efficiency (EQE) spectra of PSCs were performed on a DSR100UV-B spectrometer with a bromine tungsten light source, a SR830 lock-in amplifier and a calibrated Si detector.

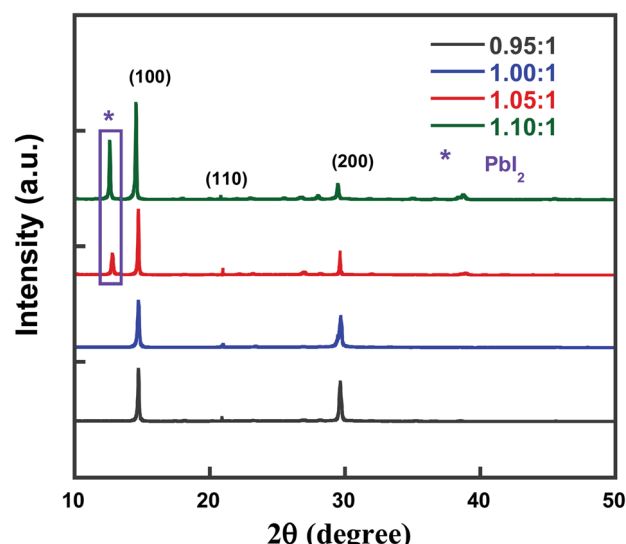


Fig. 1 The XRD patterns of perovskite thin films with different molar ratio of PbI₂ : CsBr.



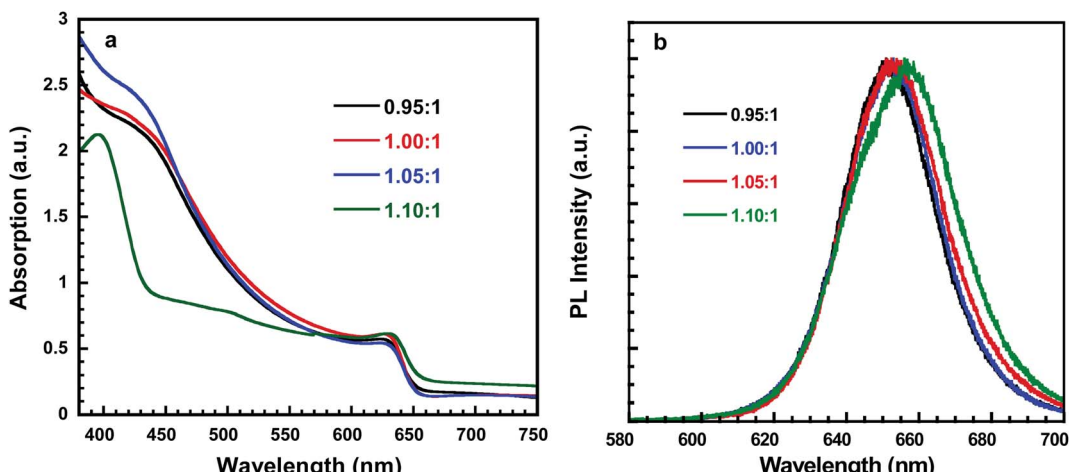


Fig. 2 (a) Absorption of perovskite thin films with different molar ratio of $\text{PbI}_2 : \text{CsBr}$. (b) Photoluminescence (PL) spectra of perovskite thin films with different molar ratios of $\text{PbI}_2 : \text{CsBr}$.

3. Results and discussion

To investigate the influence of compositional ratio of $\text{PbI}_2 : \text{CsBr}$ on the structural evolution of all-inorganic perovskite, X-ray diffraction (XRD) of these thin films are conducted in Fig. 1. Similar to perovskite with $\text{PbI}_2 : \text{CsBr}$ of 1.00 : 1, all other perovskite with $\text{PbI}_2 : \text{CsBr}$ (0.95 : 1, 1.05 : 1 and 1.10 : 1) thin

films exhibited peaks at 14.7° , 20.9° and 29.6° , which correspond to the (100), (110) and (200) crystal planes of CsPbI_2Br perovskite thin film, respectively, demonstrating prepared perovskites retain cubic phase structure, which is favorable for reducing charge recombination and promoting device performance.^{26,32} The corresponding average grain size were 61.34, 61.25, 53.75 and 55.83 nm calculated based on Scherrer

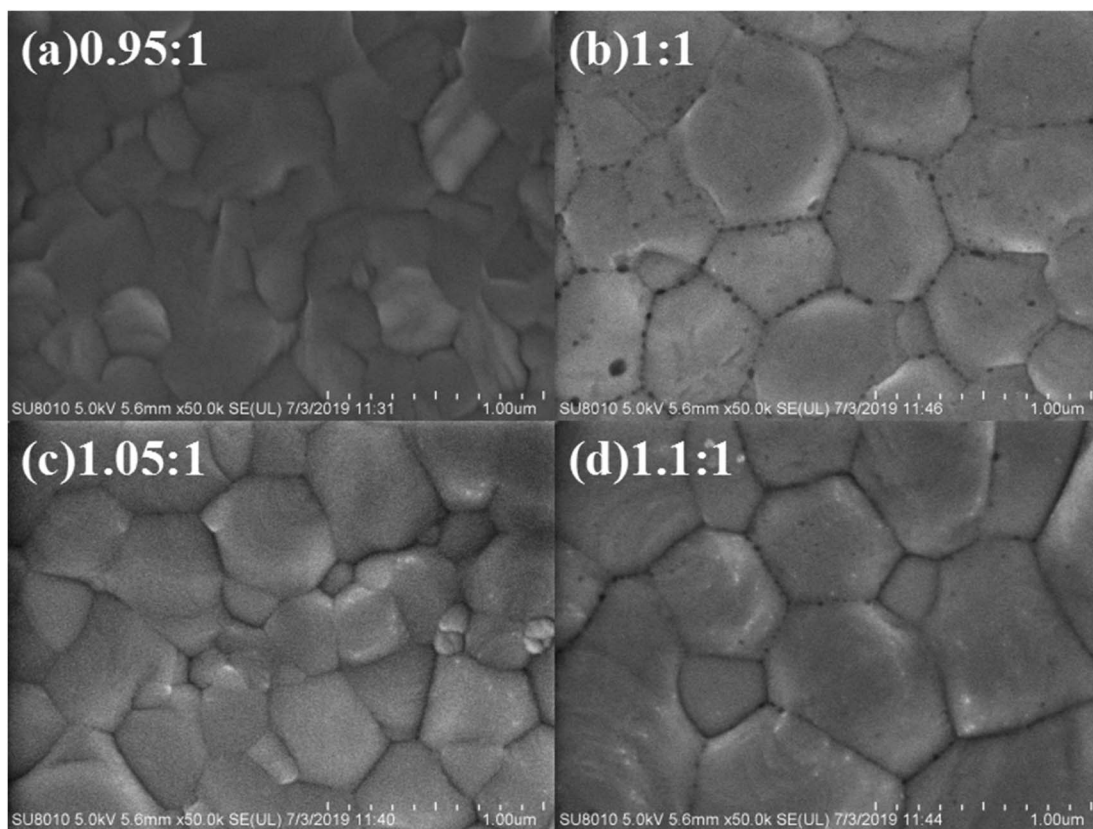


Fig. 3 (a) The top-view SEM image of CsPbI_2Br thin film with molar ratio of $\text{PbI}_2 : \text{CsBr}$ of (a) 0.95 : 1, (b) 1.00 : 1, (c) 1.05 : 1 and (d) 1.10 : 1.

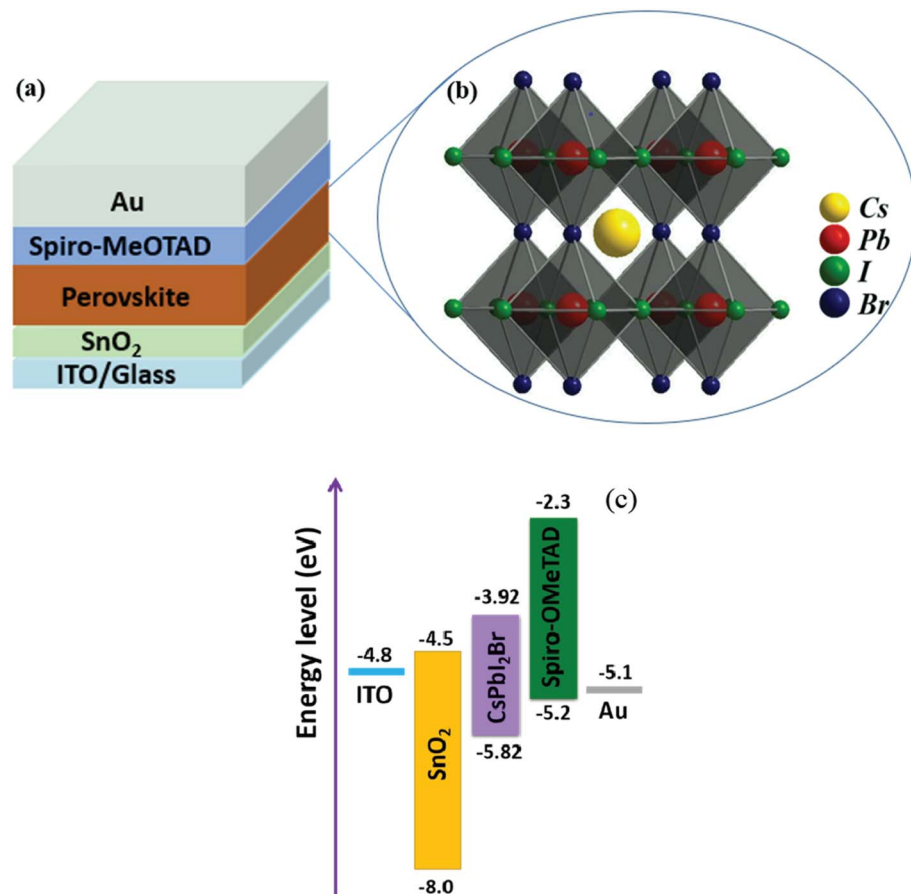


Fig. 4 (a) Device structure of the PSCs. (b) Crystal structure of the perovskite CsPbI₂Br. (c) the schematic energy diagram of glass/ITO/SnO₂/perovskite/Spiro-OMeTAD/Au device.

formula, indicating the small adjusted component ratio of the PbI₂ added into the precursor solution doesn't change crystal size significantly which is beneficial to improve the charge transport in the solar cells. The new peak located at 12.5° detected from both perovskite with PbI₂ : CsBr (1.05 : 1 and 1.10 : 1) is likely to due to the peak of excess unreacted PbI₂. It

was reported that moderate excess PbI₂ can functioned as role of passivating the surface defects for reducing the charge carrier recombination.

Fig. 2a showed the absorption spectrum of perovskite thin films, all of which exhibited the typical absorption profile for cubic phase CsPbI₂Br thin film with the typical absorption peak

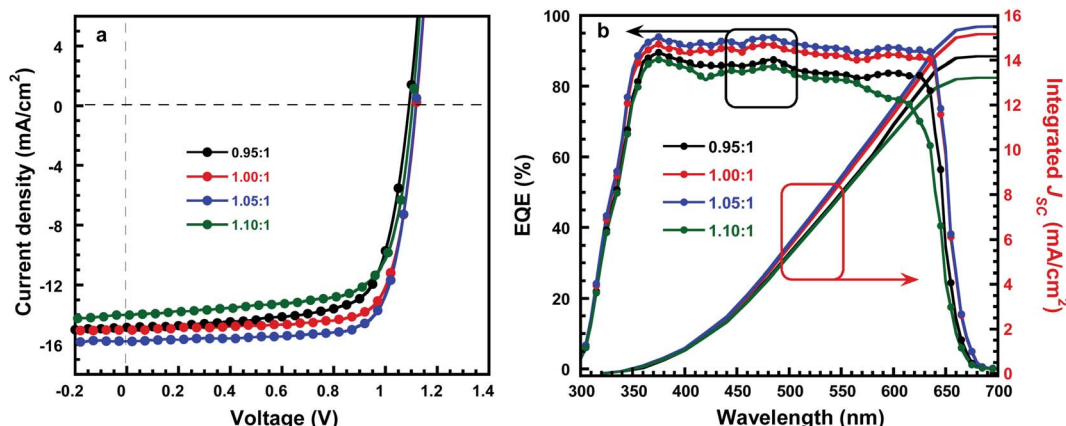


Fig. 5 (a) J - V characteristics of CsPbI₂Br thin film with molar ratio of PbI₂ : CsBr. (b) EQE spectrum and integrated J_{SC} of CsPbI₂Br thin film with molar ratio of PbI₂ : CsBr.

Table 1 Performance parameters of PSCs with different molar ratio of $\text{PbI}_2 : \text{CsBr}$

$\text{PbI}_2 : \text{CsBr}$ (molar ratio)	V_{OC} (V)	J_{SC} (mA cm^{-2})	FF (%)	PCE (%) (Best)	PCE (%) (Average)	R_s (Ωcm^2)
0.95 : 1	1.09	14.80	71.2	11.49	10.43	53.26
1.00 : 1	1.12	15.01	74.5	12.52	11.85	43.87
1.05 : 1	1.12	15.78	75.5	13.34	12.78	35.55
1.10 : 1	1.10	14.01	70.8	10.91	9.85	48.12

of 625 nm, which is consistent with other report.^{31,33} However, the perovskite film deposited with $\text{PbI}_2 : \text{CsBr}$ ratio of 1.10 : 1 has the absorption peak at 635 nm. The slightly red shifted absorption peak indicates the excess PbI_2 actually influences the CsPbI_2Br perovskite thin films. In addition, the peak is observed at 405 nm for the δ -perovskite with $\text{PbI}_2 : \text{CsBr}$ of 1.10 : 1, implying that the black α - CsPbI_2Br phase could have been partially transitioned into the yellow δ - CsPbI_2Br phase. Fig. 2b depicted the steady-state photoluminescence (PL) spectra of these four perovskite thin films. The emission peak of the CsPbI_2Br thin film is at 653 nm is well consistent with absorption edges for corresponding perovskite thin films (Fig. 2a). It is also observed that a red shifted PL peak for perovskites with the molar ratio of 1.10 : 1.

The surface morphology and crystalline size of CsPbI_2Br thin films deposited with these four different molar ratios of $\text{PbI}_2 : \text{CsBr}$ is further analyzed by SEM images, as shown in Fig. 3. It is obviously that all samples display densely stacked grains on their surfaces which is consistently with the calculated average crystal size in nanoscale range. However, brighter dots on the surface of the perovskite grains are clearly observed when the molar ratio of $\text{PbI}_2 : \text{CsBr}$ is 1.10 : 1 (Fig. 3d), proofing the existence of the unreacted PbI_2 particles could affect the thin film quality.

To investigate the effect of composition ratios of $\text{PbI}_2 : \text{CsBr}$ on the photovoltaic performance of PSCs, devices with a planar heterojunction structure of ITO/SnO₂/CsPbI₂Br/Spiro-MeOTAD/Au (Fig. 4a) with the CsPbI₂Br shown in Fig. 4b were fabricated where ITO acts as the cathode electrode, solution-processed SnO₂ thin film is used as the electron extraction layer, Spiro-MeOTAD acts as the hole extraction layer and Au acts as the anode electrode, respectively (Fig. 4c). The current densities versus voltages (J - V) characteristics of PSCs under one-sun illumination with the light intensity of 100 mW cm⁻², at the scan rate of 0.20 V s⁻¹ and the reverse scan direction, are shown in Fig. 5a. The device performance parameters are summarized in Table 1. The PSCs based on the perovskite with $\text{PbI}_2 : \text{CsBr}$ of 0.95 : 1 and 1.00 : 1 show PCE of 11.49% (V_{OC} of 1.09 V, J_{SC} of 14.8 mA cm⁻² and FF of 71.2%) and 12.52% (V_{OC} of 1.12 V, J_{SC} of 15.01 mA cm⁻² and FF of 74.5%). The PSCs based on the perovskite with $\text{PbI}_2 : \text{CsBr}$ of 1.05 : 1 shows an enhanced performance upon slightly increasing with PbI_2 . Specifically, the PCE is increased to 13.34% with a V_{OC} , J_{SC} , and FF of 1.12 V, 15.78 mA cm⁻², and 75.5%, respectively. It is worth noted that the simultaneously enhanced V_{OC} , J_{SC} and FF is achieved. These enhancements are attributed to the denser, higher crystallinity

CsPbI_2Br grains which could effectively suppress charge recombination (Fig. 3c). However, further addition of much more PbI_2 causes a negative performance change. For example, when the molar ratio of $\text{PbI}_2 : \text{CsBr}$ is increased to 1.10 : 1, the PCE is decreased to 10.91% (V_{OC} of 1.10 V, J_{SC} of 14.01 mA cm⁻², FF of 70.8%). The excess PbI_2 has reduced the sunlight absorption efficiency (Fig. 2a) and could act as recombination or trap centers with unnecessary spots on the active CsPbI_2Br thin film (Fig. 3d), severely reducing the photocurrent and FF (Table 1). The strong correlation between J_{SC} and series resistance (R_s) could be validated that with more and more PbI_2 added, the measured R_s has consistently reduced when the molar ratio changes from 0.95 to 1.05 (Table 1), indicating the improved crystallinity does increase the charge separation and carrier transport efficiency. Thus the molar ratio of $\text{PbI}_2 : \text{CsBr}$ in the precursor solution is a crucial parameter for determining device performance.

EQE of all the perovskite solar cells is shown in Fig. 5b. The perovskite solar cells exhibit a photoresponse in the wavelength ranging from 300 to 650 nm, suggesting absorbed photos being converted into charge carriers, and further generates into photocurrent in the solar cells. In addition, the champion device shows a maximum value of about 93.4% at $\lambda = 480$ nm, the integrated J_{SC} values from the EQE spectra are 14.17 mA

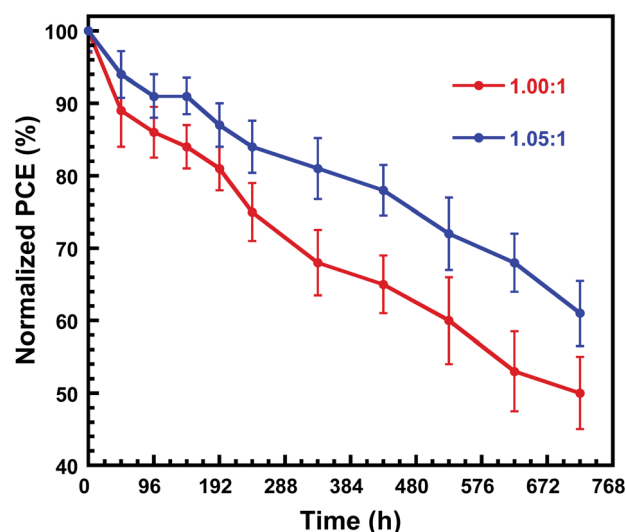


Fig. 6 Normalized PCEs of the unencapsulated PSCs fabricated by perovskite with $\text{PbI}_2 : \text{CsBr}$ of 1.00 : 1 and 1.05 : 1 functioned as the time under N_2 -filled glove box.



cm^{-2} , 15.16 mA cm^{-2} , 15.51 and 13.22 mA cm^{-2} for the PSCs fabricated by perovskite with $\text{PbI}_2 : \text{CsBr}$ of $0.95 : 1$, $1.00 : 1$, $1.05 : 1$ and $1.10 : 1$, respectively, which is about 5% error between the J_{SC} from EQE spectra and $J\text{-}V$ curve, implying the accuracy of device performance.

Furthermore, as the stability is the priority concern for the PSCs, the shelf stability of the PSCs is investigated. The devices are stored in N_2 atmosphere without any encapsulation. As shown in Fig. 6, the PSCs fabricated by perovskite with $\text{PbI}_2 : \text{CsBr}$ of $1.05 : 1$ showed a better shelf stability than that of PSCs fabricated by perovskite with $\text{PbI}_2 : \text{CsBr}$ of $1.00 : 1$. After being stored for 240 h, PSCs fabricated by perovskite with $\text{PbI}_2 : \text{CsBr}$ of $1.05 : 1$ retained 84% of the initial PCE, while the PCE of PSCs fabricated by perovskite with $1 : 1$ ratio of the two precursors dropped to 75% of the initial value in the same storage condition and time. The enhanced shelf stability which we attribute to the surface passivation of unreacted PbI_2 .³⁴⁻³⁶

4. Conclusions

In summary, we investigated the effect of compositional engineering on the film properties and device performance of inorganic perovskite CsPbI_2Br by changing the stoichiometric ratios of PbI_2 and CsBr ($0.95 : 1$, $1.00 : 1$, $1.05 : 1$ and $1.10 : 1$). The results show that the molar ratio of the raw materials is $1.05 : 1$, the CsPbI_2Br film shows the best crystallinity and the corresponding solar cell (ITO/SnO₂/CsPbI₂Br/Spiro-MeOTAD/Au) achieves the highest efficiency of 13.34%. XRD and SEM results show that once the molar ratio of raw materials is increased to $1.10 : 1$, the resultant film contains more PbI_2 , which may provide more recombination centers for free electrons and holes, thus significantly reducing the efficiency of the device. Our study highlights the importance of compositional engineering and offers a meaningful reference for the preparation of stable and efficient solar cell devices.

Conflicts of interest

There are no conflicts of interest to declare.

Acknowledgements

We thank Shenzhen Municipal Development and Reform Commission, and New Energy Technology Engineering Laboratory (Grant number: SDRC [2016]172).

References

- S. D. Stranks, G. E. Eperon, G. Grancini, C. Menelaou, M. J. Alcocer, T. Leijtens, L. M. Herz, A. Petrozza and H. J. Snaith, *Science*, 2013, **342**, 341–344.
- S. D. Stranks, V. M. Burlakov, T. Leijtens, J. M. Ball, A. Goriely and H. J. Snaith, *Phys. Rev. Appl.*, 2014, **2**, 034007.
- C. S. Ponseca Jr, T. J. Savenije, M. Abdellah, K. Zheng, A. Yartsev, T. Pascher, T. Harlang, P. Chabera, T. Pullerits and A. Stepanov, *J. Am. Chem. Soc.*, 2014, **136**, 5189–5192.
- Q. Dong, Y. Fang, Y. Shao, P. Mulligan, J. Qiu, L. Cao and J. Huang, *Science*, 2015, **347**, 967–970.
- D. Shi, V. Adinolfi, R. Comin, M. Yuan, E. Alarousu, A. Buin, Y. Chen, S. Hoogland, A. Rothenberger and K. Katsiev, *Science*, 2015, **347**, 519–522.
- M. A. Green, A. Ho-Baillie and H. J. Snaith, *Nat. Photonics*, 2014, **8**, 506–514.
- J.-P. Correa-Baena, A. Abate, M. Saliba, W. Tress, T. Jesper Jacobsson, M. Grätzel and A. Hagfeldt, *Energy Environ. Sci.*, 2017, **10**, 710–727.
- S. Gholipour and M. Saliba, *Small*, 2018, **14**, e1802385.
- Laboratory, T. N. R. E., <https://www.nrel.gov/pv/cell-efficiency.html>, 2019.
- T. Leijtens, G. E. Eperon, N. K. Noel, S. N. Habisreutinger, A. Petrozza and H. J. Snaith, *Adv. Energy Mater.*, 2015, **5**, 1500963.
- B. W. Park and S. I. Seok, *Adv. Mater.*, 2019, **31**, e1805337.
- T. A. Berhe, W.-N. Su, C.-H. Chen, C.-J. Pan, J.-H. Cheng, H.-M. Chen, M.-C. Tsai, L.-Y. Chen, A. A. Dubale and B.-J. Hwang, *Energy Environ. Sci.*, 2016, **9**, 323–356.
- Q. Fu, X. Tang, B. Huang, T. Hu, L. Tan, L. Chen and Y. Chen, *Adv. Sci.*, 2018, **5**, 1700387.
- Z. Zhao, F. Gu, H. Rao, S. Ye, Z. Liu, Z. Bian and C. Huang, *Adv. Energy Mater.*, 2019, **9**, 1802671.
- W. Ahmad, J. Khan, G. Niu and J. Tang, *Sol. RRL*, 2017, **1**, 1700048.
- G. E. Eperon, G. M. Paternò, R. J. Sutton, A. Zampetti, A. A. Haghaghirad, F. Cacialli and H. J. Snaith, *J. Mater. Chem. A*, 2015, **3**, 19688–19695.
- Q. Zeng, X. Zhang, C. Liu, T. Feng, Z. Chen, W. Zhang, W. Zheng, H. Zhang and B. Yang, *Sol. RRL*, 2019, **3**, 1800239.
- H. Yuan, Y. Zhao, J. Duan, Y. Wang, X. Yang and Q. Tang, *J. Mater. Chem. A*, 2018, **6**, 24324–24329.
- P. Zhu, C. Chen, S. Gu, R. Lin and J. Zhu, *Sol. RRL*, 2018, **2**, 1700224.
- Q. Tai, K.-C. Tang and F. Yan, *Energy Environ. Sci.*, 2019, 2375–2405.
- Y. Zhou and Y. Zhao, *Energy Environ. Sci.*, 2019, **12**, 1495–1511.
- C. Dong, X. Han, W. Li, Q. Qiu and J. Wang, *Nano Energy*, 2019, **59**, 553–559.
- Y. Chen, T. Shi, P. Liu, W. Xie, K. Chen, X. Xu, L. Shui, C. Shang, Z. Chen, H.-L. Yip, G. Zhou and X. Wang, *J. Mater. Chem. A*, 2019, **7**, 20201–20207.
- L. Zhou, X. Guo, Z. Lin, J. Ma, J. Su, Z. Hu, C. Zhang, S. Liu, J. Chang and Y. Hao, *Nano Energy*, 2019, **60**, 583–590.
- S. Zhang, S. Wu, W. Chen, H. Zhu, Z. Xiong, Z. Yang, C. Chen, R. Chen, L. Han and W. Chen, *Materials today energy*, 2018, **8**, 125–133.
- G. Yin, H. Zhao, H. Jiang, S. Yuan, T. Niu, K. Zhao, Z. Liu and S. F. Liu, *Adv. Funct. Mater.*, 2018, **28**, 1803269.
- Y. Guo, F. Zhao, J. Tao, J. Jiang, J. Zhang, J. Yang, Z. Hu and J. Chu, *ChemSusChem*, 2019, **12**, 983–989.
- D. Bai, H. Bian, Z. Jin, H. Wang, L. Meng, Q. Wang and S. F. Liu, *Nano energy*, 2018, **52**, 408–415.
- W. Chen, H. Chen, G. Xu, R. Xue, S. Wang, Y. Li and Y. Li, *Joule*, 2019, **3**, 191–204.



30 C. Liu, W. Li, C. Zhang, Y. Ma, J. Fan and Y. Mai, *J. Am. Chem. Soc.*, 2018, **140**, 3825–3828.

31 C. Dong, X. Han, W. Li, Q. Qiu and J. Wang, *Nano Energy*, 2019, **59**, 553–559.

32 J. K. Nam, M. S. Jung, S. U. Chai, Y. J. Choi, D. Kim and J. H. Park, *J. Phys. Chem. Lett.*, 2017, **8**, 2936–2940.

33 Z. Zhang, J. Zhang, X. Gan, H. Sun, M. Shang, D. Hou, C. Lu, R. Chen, Y. Zhu and L. Han, *Adv. Energy Mater.*, 2018, **8**, 1801050.

34 Y. Zhao, Q. Li, W. Zhou, Y. Hou, Y. Zhao, R. Fu, D. Yu, X. Liu and Q. Zhao, *Sol. RRL*, 2019, **3**, 1800296.

35 D. H. Cao, C. C. Stoumpos, C. D. Malliakas, M. J. Katz, O. K. Farha, J. T. Hupp and M. G. Kanatzidis, *APL Mater.*, 2014, **2**, 091101.

36 S. Wang, W. Dong, X. Fang, Q. Zhang, S. Zhou, Z. Deng, R. Tao, J. Shao, R. Xia and C. Song, *Nanoscale*, 2016, **8**, 6600–6608.

